Vibrational and structural signatures of the crossover between dense glassy and sparse gel-like attractive colloidal packings

Matthew A. Lohr,[1,*] Tim Still,[1,*] Raman Ganti,[1] Matthew D. Gratale,[1] Zoey S. Davidson,[1] Kevin B. Aptowicz,[2] Carl P. Goodrich,[1] Daniel M. Sussman,[1] and A. G. Yodh[1]

[1]*Department of Physics and Astronomy, University of Pennsylvania, Philadelphia, Pennsylvania 19104, USA*

[2]*Department of Physics, West Chester University, West Chester, Pennsylvania 19383, USA*

(Received 16 July 2014; revised manuscript received 10 October 2014; published 5 December 2014)

We investigate the vibrational modes of quasi-two-dimensional disordered colloidal packings of hard colloidal spheres with short-range attractions as a function of packing fraction. Certain properties of the vibrational density of states (vDOS) are shown to correlate with the density and structure of the samples (i.e., in sparsely versus densely packed samples). Specifically, a crossover from dense glassy to sparse gel-like states is suggested by an excess of phonon modes at low frequency and by a variation in the slope of the vDOS with frequency at low frequency. This change in phonon mode distribution is demonstrated to arise largely from localized vibrations that involve individual and/or small clusters of particles with few local bonds. Conventional order parameters and void statistics did not exhibit obvious gel-glass signatures as a function of volume fraction. These mode behaviors and accompanying structural insights offer a potentially new set of indicators for identification of glass-gel transitions and for assignment of gel-like versus glass-like character to a disordered solid material.

DOI: 10.1103/PhysRevE.90.062305 PACS number(s): 64.70.pv, 64.70.kj, 63.20.Pw, 63.50.Lm

I. INTRODUCTION

Though gels are a common component of consumer products and biological systems, they are a poorly defined state of matter [1]. The term "gel" is used to describe virtually any low-density, spatially heterogeneous disordered material with solid-like properties. Such materials form from collections of particles with sufficiently strong attraction, including colloidal particles in polymer solutions that aggregate via depletion forces [2], clay disks with anisotropic electrostatic interactions [3], and carbon nanotubes in solution [4]. The morphology of these structures depends on details of their interparticle interactions and assembly dynamics [1], and as a result of these underlying complexities, a single unifying physical description of gels has been elusive.

Glasses, or disordered dense solid packings, are better characterized states of matter than gels. Nevertheless, the underlying physics of glassy materials is still an active area of research with many open questions [5–7]. Recent theoretical and experimental work has used the observation of vibrational modes in these systems to characterize the approach to the unjamming transition [8–11], and to predict the location of rearrangement-prone regions [12–17]. Insights derived from vibrational modes, however, have typically been limited to dense glassy packings of particles with repulsive interactions, i.e., repulsive glasses. Glassy packings of particles with attractive interactions, i.e., attractive glasses, are structurally and dynamically different from repulsive glasses [18–22] and have vibrational properties which are not as well studied.

Here we carry out experiments which aim to distinguish gels from attractive glasses, especially in the crossover regime of intermediate density. Generally, no obvious structural differences distinguish a very dense gel from a porous attractive glass. Distinguishing gels and glasses based on dynamics is also difficult, since gels share several characteristic traits of glassy materials, such as dynamical heterogeneity [23], and a prevalence of low-frequency vibrational modes compared to crystalline solids [11,24]. Recent efforts to characterize the crossover from attractive glasses to gels have focused on two-step rheological yielding [25], changes in time scales of slow relaxation processes [26], scaling of bulk elastic properties [27], and deviations of a phase boundary line from percolation theory [28]. However, a distinct microstructural or localized dynamical signature of the gel-to-glass crossover has not yet been observed in "static" samples, e.g., in unsheared ensembles of strongly attractive particles. Such a distinction could facilitate identification of materials with gel-like versus glass-like properties without significant perturbation of the sample.

Experiments in this contribution aim to distinguish gel-like and glassy states by exploring packing-fraction-driven changes in the vibrational modes of quasi-two-dimensional, dynamically arrested, thermal samples of colloidal particles with attractive interactions. When the sample packing fraction is decreased below a particular value, we observe a marked increase in the number of low-frequency modes of the sample's vibrational density of states (vDOS) and a marked change in the slope of the vDOS versus frequency at low frequencies. These behaviors differ from those that are qualitatively expected for attractive glassy packings. Therefore, we suggest that these vDOS features can serve as a marker of gel-like vibrational behavior. Further, we find that these low-frequency modes are predominantly associated with particles that have low local coordination. Such localization is qualitatively similar to the localization of transverse modes to poorly coordinated particles, as observed in simulations of very dilute gels [24].

The appearance of these localized vibrational modes thus suggests that gel-like packings may be distinguished from glassy packings via unique microstructural features. The mode behaviors and accompanying structural insights offer a potentially new set of indicators for identification of glass-gel transitions and/or for assignment of gel-like versus glass-like

[*]M.A.L. and T.S. contributed equally to this work.

character to a disordered solid material. In addition to vDOS, we investigate the variation of void properties and distributions, as well as a range of conventional order parameters and correlation functions; none of these exhibit obvious gel-glass signatures as a function of volume fraction.

II. EXPERIMENTAL DETAILS AND METHODS

We create dense attractive colloidal monolayers in a manner that ensures observable Brownian motion. Bidisperse suspensions of 1.0 and 1.4 μm carboxyl-modified polystyrene (PS) colloidal spheres (Invitrogen) in a 1:1 number ratio are suspended in a mixture of water and 2,6-lutidine near its critical composition, i.e., with a lutidine mass fraction of 0.28. At a critical temperature of 306.5 K, this solvent mixture induces a wetting-mediated short-range attractive interaction between particles with a strength of $\approx 4\ k_B T$ [29–33]. We load dilute suspensions of these particles (1% wt/wt) between two hexamethyldisilazane (HMDS) functionalized glass cover slips separated by a 25-μm spacer. This sample is then placed on an inverted microscope with an oil-immersion objective that can be heated to the colloidal aggregation temperature using a high-temperature stability objective heater (Bioscience Tools).

By carefully cycling the temperature of the sample into and out of the colloidal aggregation regime, we create monolayers of particles on the bottom surface of the cell that are stabilized by a corresponding weak attraction to the wall. After acquiring bright-field microscopy video of the resulting monolayers at 60 frames per second, we employ subpixel particle tracking algorithms [34] to calculate each particle's trajectory within a 60×80 μm section of the packing (1500–3000 particles, depending on ϕ). We characterize the structure and dynamics of these stable monolayer packings from these trajectories.

Depending on the initial concentration of colloids in suspension, the resulting monolayer packing can range from a sparse, barely percolating structure with area fraction $\phi = 0.50 \pm 0.01$, to a homogeneous, dense packing with $\phi = 0.84 \pm 0.01$, as shown in Figs. 1(a)–1(f). The use of water-lutidine based wetting rather than a depletion-induced attraction enables us to keep the viscosity of the solvent low, which minimizes damping in the packings. Additionally, by forming the packing on the bottom surface of a larger cell (i.e., instead of confining it in cells of thickness close to a single particle diameter), we reduce damping effects from confinement, and we avert changes in water-lutidine phase behavior, which are sometimes observed in confined geometries.

III. RESULTS AND DISCUSSION

A. MSD and structure

Thirteen different packings with area fractions ranging from $0.50 \leqslant \phi \leqslant 0.84$ were examined. We first discuss the structure and traditional displacement dynamics. Discontinuous changes in average structural properties are not apparent among the dense, spatially homogeneous (which we later identify as glass-like) and the sparse, spatially heterogeneous (later identified as gel-like) packings. Though the packings become continuously more spatially heterogeneous with decreasing ϕ [see Figs. 1(a)–1(f)], a substantive change in common structural measures is not apparent. For example, the pair correlation functions, $g(r)$, remain qualitatively similar [see Fig. 1(g)]; specifically, the peak positions at one to two particle separations, and up to several particle lengths, are the same for all samples within our measurement error. Thus, if a structural hallmark of the gel-to-glass crossover exists, it is hidden from view in $g(r)$. The narrow width of the first peaks in $g(r)$ reflects the relatively small polydispersity of our particles (3% or smaller) and gives us further confidence about the quality of the particle tracking (see Supplemental Material [35]).

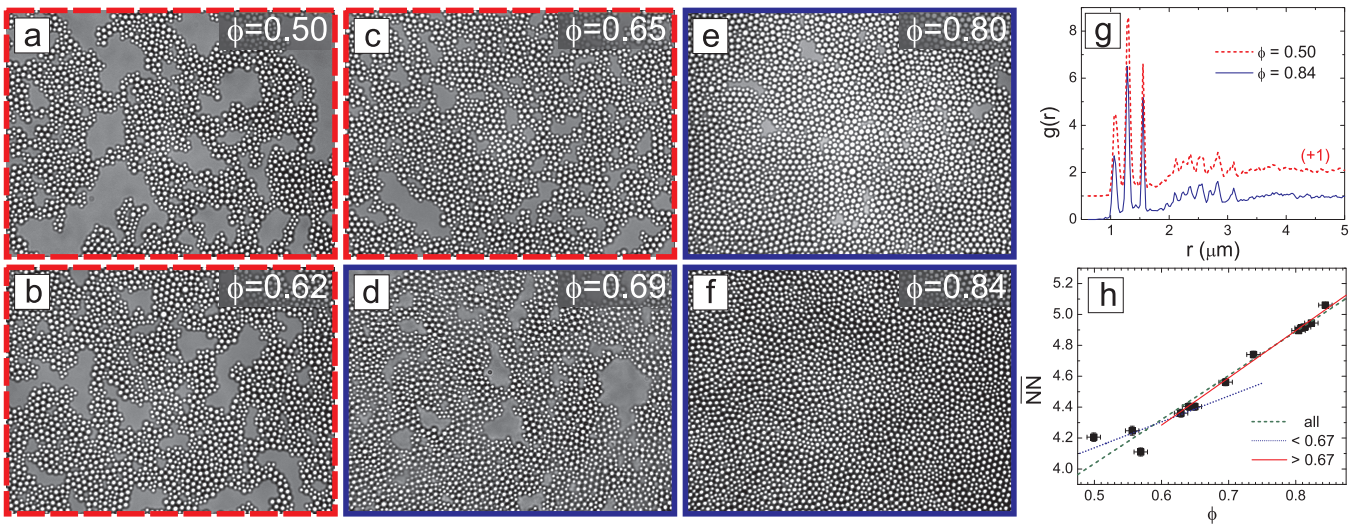

FIG. 1. (Color online) Bright-field microscopy images of bidisperse attractive PS monolayer packings at various densities, with contrast and brightness enhancement for clarity, and with total area fractions of (a)–(f) $0.50 \leqslant \phi \leqslant 0.84$ (all ± 0.01); gel-like packings [$\phi < 0.67$, (a)–(c), see text] have a dashed red frame. The field of view is approximately 60×80 μm. (g) Pair correlation function $g(r)$ of the most dense ($\phi = 0.84$, blue solid line) and most sparse ($\phi = 0.50$, red dotted line, shifted by +1.0) packings. Note that $g(r)$ is normalized by the particle number density; therefore, the magnitudes of the first peaks are not directly proportional to the packing fraction ϕ. (h) Average number of nearest neighbors, $\overline{\mathrm{NN}}$, as a function of ϕ. See text for discussion of linear fits.

In a different vein, we measured the particle mean squared displacement (MSD) as a function of volume fraction (see Supplemental Material [35]). The MSD data at the different volume fractions were somewhat noisy, but they exhibited similar temporal trends without distinct or sharp features that might signal differences between gel and glass states.

We also studied the average number of nearest neighbors. Here, nearest neighbors are defined as particle pairs with spatial separations closer than the distance set by the dip just after the third peak in $g(r)$. The average number of nearest neighbors per particle, $\overline{\mathrm{NN}}$, increases roughly monotonically with volume fraction [Fig. 1(h)]. This behavior is expected (on average), since the total perimeter on the voids should decrease with increasing particle packing fraction (on average). Interestingly, when all samples are included, the data is fit reasonably well by a single line with slope 2.9 ± 0.6 [dashed line in Fig. 1(h)].

We next exhibit the distribution of void areas and void perimeters in the 13 samples. (Note that only those voids whose size was comparable to or larger than the area occupied by a single small particle are included in the analysis.) Broadly speaking, the void data do not exhibit any behaviors that can be interpreted as a gel-glass crossover transition. The most important findings are summarized in Fig. 2. In Fig. 2(a), we show the number of voids, N_v, for all samples. As one would expect, N_v generally decreases with increasing ϕ. For every individual void, we also measure the void perimeter, P_v, and void area, A_v. Interestingly, the measured P_v versus A_v follows a power law when data from all ϕ are included [see Fig. 2(b)]. We next computed the total area and total perimeter of all voids in each sample. Figures 2(c) and 2(d) plot these parameters, i.e., $\sum A_v$ and $\sum P_v$, respectively, as a function of ϕ. As expected, $\sum A_v$ decreases linearly with ϕ (on average). $\sum P_v(\phi)$ varies in a similar way with ϕ (on average), with one exception; in the sample with the volume fraction, $\phi \approx 0.50$, the total void perimeter is considerably smaller than the $\sum P_v$ of samples with slightly higher packing fractions. We believe this deviation from average behavior is a statistical anomaly due to a greater number of large voids in this particular sample (see Supplemental Material) [35]. In fact, the consequence of this behavior is also apparent in our nearest neighbor data (see discussion below).

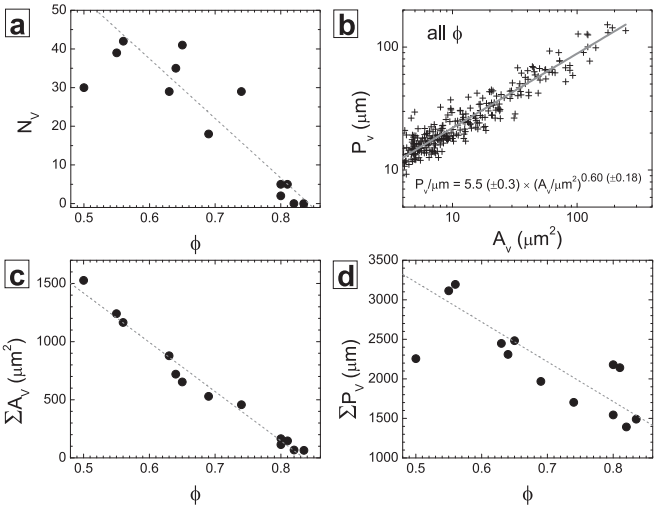

FIG. 2. Void statistics for all voids larger than the size of a single particle. (a) Number of voids, N_v, as a function of ϕ; the line is a guide for the eye. (b) Void perimeter, P_v, as a function of void area, A_v, for all voids and all ϕ. The solid line shows a power law fit. (c) Total void area, $\sum A_v$, as a function of ϕ with linear fit. (d) Total void perimeter, $\sum P_v$ as a function of ϕ; the line is a guide for the eye.

B. Vibrational mode analysis

Interestingly, differences between sparse and dense packings can be readily identified in their vibrational mode spectra. Here we follow previous work in order to calculate vibrational modes of these samples from particle trajectories [11,36–38]. We first calculate the time-averaged covariance matrix $C_{ij} = \langle u_i(t) u_j(t) \rangle_t$, where $u_i(t)$ are particle displacements from their average positions. In the harmonic approximation, the covariance matrix is directly related to the matrix of effective spring constants, K, connecting particles in an undamped "shadow" system, i.e., by $(C^{-1})_{ij} k_B T = K_{ij}$. The dynamical matrix of this "shadow" system, D, is related to K; i.e., $D_{ij} = K_{ij}/m_{ij}$, where $m_{ij} = \sqrt{m_i m_j}$ is the reduced mass and m_i is the mass of particle i. The eigenvalues of the dynamical matrix give the squared frequencies of vibrational modes of the system, ω^2, and the corresponding eigenvector components, $\vec{e}_i(\omega)$, represent the displacement amplitudes of the given vibrational mode at particle i.

We calculate the mode eigenfrequencies and eigenvectors for the 13 packings, using $N_f = 10^4$ frames for each packing. In carrying out this procedure we perform a fit, described in detail in previous work, that adjusts the high-frequency mode frequencies to their expected values (i.e., calculated from an infinitely long time track) which are shifted due to finite statistics [39–42].

Per tracking, an important processing step, which helps avoid anomalous shifting of particle position due to image overlap, is to set the correct value for the anticipated particle diameter when applying the band-pass filter to identify particles. Per noise effects more broadly, we tested for the influence of positional noise by adding random noise to the particle positions in the data; the effect of this noise was sometimes evident in the vDOS at high phonon frequency, but it did not affect the low-frequency vDOS, which are used to distinguish gels from glasses. (Note that many of these issues have been explicitly addressed in Ref. [40].) Finally, we remind the reader that it is important that particle rearrangements do not occur in the data streams we use to compute the vDOS, i.e., that the packing is in a "permanent" potential. Sparsely packed samples are more susceptible to this issue than densely packed samples, but the fact that all particles are bound to one another via strong attractive interactions has an overall effect that tends to reduce particle mobility compared to samples with largely repulsive interactions (i.e., even on the void perimeter). Nevertheless, a small number of excursions could occur. To this end, we measured all systems for 10^5 frames, and we only analyzed intervals of 10^4 consecutive frames, wherein, to the best of our ability, we were unable to discern rearrangements. We also carried out several tests to identify candidate particles for large motions (in the six gel-like samples, about 30 particles were found to move >100 nm and were correlated with a large

amplitude localized modes) and to ascertain their possible effects. We computed the vDOS with and without all particles that moved >100 nm. The vDOS data remain essentially the same (see figure in Supplemental Material) [35], and even the minor differences observed are likely a result of variation in total number of eigenmodes (due to different numbers of particles in each sample).

The resulting vDOS exhibits a pronounced variation in the distribution of low-frequency modes with respect to changes in packing fraction [Fig. 3(a)]. While all vDOS plots show a peak at the mean frequency, $\bar{\omega}$, and a plateau at slightly lower frequencies ($0.1 < \omega/\bar{\omega} < 0.4$), distinct behaviors are seen at the lower frequencies ($\omega/\bar{\omega} < 0.1$). Notably, the slope of the vDOS with respect to frequency, ω, varies both in magnitude and in sign at low frequencies as a function of volume fraction. Further, a substantial increase in the relative number of modes is evident in the sparser packings ($\phi < 0.67$) at low frequency; this effect is suggestive of a possible crossover from a glassy to a gel-like state.

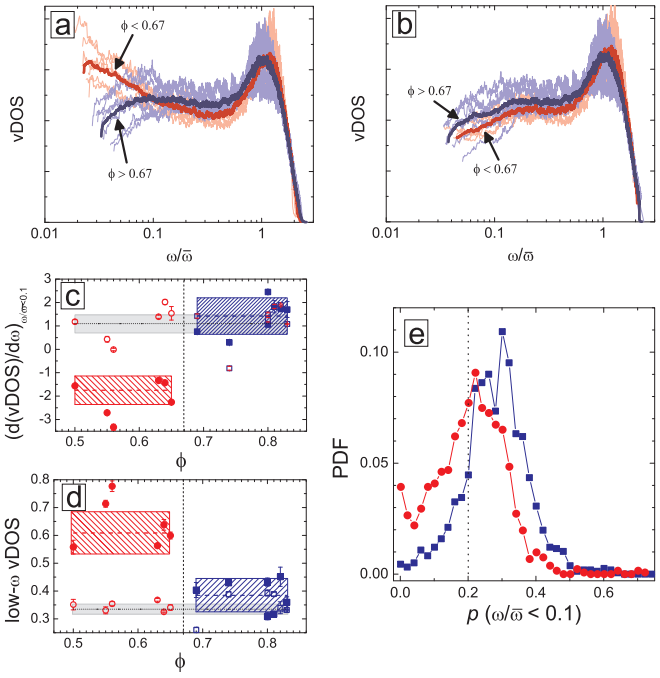

FIG. 3. (Color online) (a), (b) Vibrational density of states as a function of frequency, w, calculated from the eigenmode distributions in packings with $\phi < 0.67$ (i.e., six packings with $\phi = 0.50$, 0.55, 0.56, 0.62, 0.64, and 0.65, each ± 0.01) (red lines) and $\phi > 0.67$ (i.e., seven packings with $\phi = 0.69$, 0.74, 0.80, 0.80, 0.81, 0.82, and 0.84, each ± 0.01) (blue lines). Thin, faded lines indicate vDOS for individual packings; thicker lines are the average vDOS for all packings in the sparse ($\phi < 0.67$, red) and dense ($\phi > 0.67$, blue) regimes. Panel (a) shows vDOS curves calculated from all modes; (b) shows vDOS curves calculated discounting highly localized modes ($p < 0.2$). (c) Low-frequency slope of vDOS (for $\omega/\bar{\omega} \leqslant 0.1$) as a function of ϕ counting all modes [from (a), solid symbols] and discounting highly localized modes [from (b), open symbols]. Horizontal lines and boxes show average values and standard deviations for gel-like ($\phi < 0.67$) and glass-like ($\phi > 0.67$) systems using all modes, as well as for all ϕ but discounting highly localized modes. (d) Low-frequency value of vDOS as a function of ϕ counting all modes [from (a), solid symbols] and discounting highly localized modes [from (b), open symbols]. Horizontal lines and boxes are used analogous to those in (c). (e) Histogram of participation ratio $p(\omega/\bar{\omega} < 0.1)$ for packings with $\phi < 0.67$ (open red squares) and $\phi > 0.67$ (solid blue squares).

More specifically, for all packings with $\phi > 0.67$, the density of states decreases with decreasing frequency, while for all packings with $\phi < 0.67$, the vDOS increases with decreasing frequency. The general shape of the vDOS curve for denser packings qualitatively resembles the vDOS for model packings slightly above the jamming transition [8–10]; it has a high-frequency peak, a plateau at intermediate frequencies (which, in our experiments, fall in the range of $0.1 < \omega/\bar{\omega} < 0.4$), and a dropoff below a characteristic frequency, $\omega^{\star}$. Since our theoretical understanding of the low-frequency behavior depends on the assumption that spatial fluctuations are suppressed [43], this result might be expected for the densest, spatially uniform (but disordered) packings. However, it is surprising that this result extends to samples with observable gaps, holes, and spatial heterogeneity larger than a single particle diameter ($0.69 < \phi < 0.80$). We thus describe all packings that exhibit this downturn in low-ω vDOS as exhibiting "dense" or "glassy" behavior.

The vDOS of sparser packings ($\phi < 0.67$) is increasing for $\omega/\bar{\omega} < 0.1$, and it therefore does not closely resemble a conventional glassy mode distribution at low frequencies. In simulations of uniform glassy packings in stable "lowest density" configurations, a dropoff at low frequencies is not always observed [8–10]. Instead, in these simulations, the plateau value at intermediate frequencies extends to arbitrarily low frequencies near the unjamming transition. An increase in vDOS *above* this plateau value is therefore not predicted from the behavior of purely repulsive glasses, nor easily understood in the context of spatially homogeneous packings. We thus ascribe these packings that exhibit an upturn to have "sparse" or "gel-like" vDOS behavior.

Additionally, the low-frequency vDOS curves have similar slopes for both all sparse ($\phi < 0.67$) and all dense ($\phi > 0.67$) packings, respectively. Within these groups, obvious monotonic changes as a function of ϕ are not readily apparent. These observations suggest that the appearance of additional low-frequency modes might not be *directly* related to continuous changes in density, coordination number, and/or spatial heterogeneity.

C. Localization of signature gel-like modes

Quantification of the spatial distribution of low-frequency modes provides insight into the structural nature of the ϕ-mediated change in the vDOS curve. We find the localization of each mode by calculating its participation ratio, $p(\omega) = [\sum_i |\vec{e}_i(\omega)|^2]^2/[\sum_i |\vec{e}_i(\omega)|^4]$. This parameter has a value close to or greater than 0.5 for extended modes, and has lower values when modes are localized. When we compare the distributions of p in low-frequency modes ($\omega/\bar{\omega} < 0.1$) for different ϕ, we find that the sparser packings have more modes with lower p [Fig. 3(c)]. Equivalently, these sparser packings have more highly localized low-frequency modes than their denser counterparts. To determine how these highly

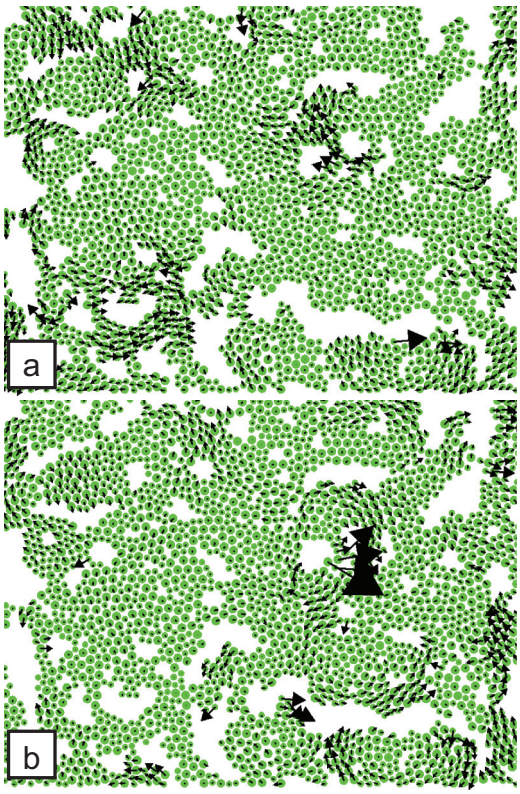

FIG. 4. (Color online) Plots of particle locations from a sparse packing ($\phi = 0.64 \pm 0.01$) overlaid with polarization eigenvector components corresponding to two modes with similar frequency [$\omega/\bar{\omega} = 0.019$ (a) and 0.021 (b)] and significantly different localization [$p = 0.32$ (i.e., a more extended mode) (a) and $p = 0.069$ (i.e., a more localized mode) (b)].

localized modes contribute to the shape of the vDOS curves, we recalculate the density of states for both sparse and dense packings, neglecting all modes with a $p < 0.2$ [Fig. 3(b)]. While the shape of the vDOS curves for dense packings remains largely unchanged, the low-frequency vDOS increase observed in sparse packings disappears, yielding curves similar in shape to those of the denser packings. This observation implies that the deviation of low-frequency modes from typical glassy behavior comes from the occurrence of highly localized vibrational modes.

By closely examining the distribution and placement of the localized vibrations in sparse packings, we gain insight into the structural features unique to packings which deviate from glassy vibrational behavior. We observe a qualitative difference in the spatial distributions of modes with similar frequencies but different participation ratios (Fig. 4). Specifically, a mode with lower p appears concentrated to a few particles with large local participation. In other words, particle vibrations in low p modes appear to be localized to small clusters. Modes with higher p (in this low-frequency range) appear slightly localized, but not nearly to the extent observed in low p modes.

With this notion of localized low-frequency modes in mind, we further consider the vDOS data. The two regimes and the crossover from glass-like to gel-like packings is emphasized in Figs. 3(c) and 3(d), where we show the low-frequency vDOS slopes and vDOS values of all curves in Fig. 3(a) (solid symbols) and 3(b) (open symbols) as a function of packing fraction. These data separate into two regimes. When all data are included, packings with $\phi < 0.67$ have low-frequency vDOS slopes of -1.8 ± 0.6 and vDOS values of 0.61 ± 0.08, and packings with $\phi > 0.67$ have low-frequency vDOS slopes of $+1.4 \pm 0.8$ and vDOS values of 0.38 ± 0.06. Furthermore, when the highly localized modes are removed from all data, packings of all ϕ assume approximately constant values of $+1.1 \pm 0.4$ for the low-frequency vDOS slopes and 0.33 ± 0.02 for vDOS values. Note that the error bars for all ϕ, after removing highly localized modes, are much smaller than the error bars of both the gel-like and glass-like states using all modes. Taken together, these data are consistent with a two-state model and a crossover transition from gel to glass at $\phi = 0.67$. Note also that, though the within-group scatter of data with ϕ was substantial, the limiting behaviors of the two different groups is clearly apparent.

For completeness, we also explored whether these data might be explained by a mixture model, rather than a two-state gel-glass model. In the mixture model, each experimental system is assumed to be a mixture of glass-like and gel-like states with a relative weighting of glass-to-gel that varies smoothly (e.g., linearly) with volume fraction. In this case, the vDOS signatures might be expected to vary linearly with sample volume fraction. In fact, it is possible to fit these data linearly with slopes of 13.8 ± 8.3 and -1.3 ± 0.6 for the data shown in Figs. 3(c) and 3(d), respectively. While a linear fitting of these data is possible, the quality of fit is comparatively low (as indicated by the given error bars, i.e., standard deviations). Nevertheless, while we believe that the data supports the crossover from gel-like to glassy states and the importance of localized modes, the data cannot unambiguously rule out either model.

Returning to the issues of localized modes, we attempt to elucidate localization effects more quantitatively by considering the distribution of single-particle eigenvector component magnitudes, $|\vec{e}_i|$. These distributions for extended ($p > 0.2$) and localized ($p < 0.2$) modes at low frequencies ($\omega/\bar{\omega} < 0.1$) are plotted in Fig. 5(a).

While all modes show a virtually identical distribution for $|\vec{e}_i| \leqslant 0.1$, the localized modes show a significantly higher probability of high-magnitude vibrations $|\vec{e}_i| \geqslant 0.1$, clearly deviating from the essentially exponential behavior seen in extended modes. These distributions of particle participations suggest that the modes which cause deviations from glassy behavior in sparse packings are "dominated" by the vibrations of just a few particles.

The local structure of the particles that dominate low-frequency modes in sparse packings provides insight into a possible microstructural signature of gel-like packings. In Fig. 5(d), we plot the distribution of cluster sizes of these particles. For the most part, it appears these modes are dominated by single particles, or clusters smaller than a few particles. More telling of the structure surrounding these particles is their local bond number. A histogram of the coordination numbers of all sparse packings, compared to the local bonding number of particles dominating localized

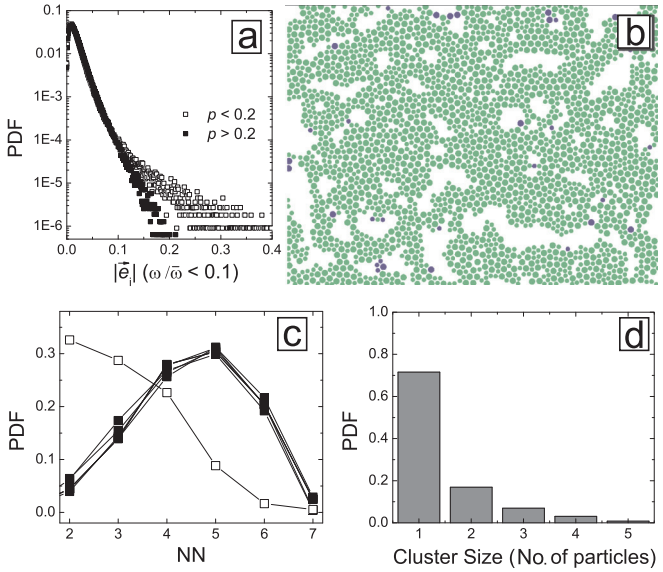

FIG. 5. (Color online) Localization of low-frequency modes in sparse packings. (a) Histograms of $|\vec{e}_i(\omega)|$ for all modes with $\omega/\bar{\omega} < 0.1$ in all observed packings with $\phi < 0.67$ for extended ($p > 0.2$, solid squares) and localized ($p < 0.2$, open squares) modes. (b) Plot of particle locations in a $\phi = 0.64 \pm 0.01$ packing, with dark blue particles significantly contributing ($|\vec{e}_i(\omega)| > 0.2$) to low-frequency modes ($\omega/\bar{\omega} < 0.1$). (c) Histogram of nearest neighbors per particle of each packing with $\phi < 0.67$ (black points) and for particles in all sparse packings that dominate a low-frequency mode (open squares, $|\vec{e}_i(\omega)| > 0.2, \omega_n/\bar{\omega} < 0.1$). (d) Histogram of the number of particles in a cluster that dominates a low-frequency mode in sparse packings ($|\vec{e}_i(\omega)| > 0.2, \omega_n/\bar{\omega} < 0.1, \phi < 0.67$).

low-frequency modes, shows that these dominating particles have relatively low coordination, with a peak at $NN = 2$ [Fig. 5(c)].

The localization of low-energy vibrational modes at particles with low coordination is a result consistent with basic intuition and with recent work on vibrational modes in related systems [24,30,31,44]. Fewer constraining bonds on a particle lead to lower confining energies, which would logically result in lower-frequency localized modes. Additionally, experimental work has shown that the mean frequency of modes in small colloidal clusters scales with their average coordination number [30]. Similarly, recent simulations of sparse gels of particles with limited valences demonstrate an increase in low-frequency modes in packings with increasing sparsity, which is related to the appearance of low-energy transverse vibrations in linear particle chains [24]. By highlighting particles which dominate localized low-frequency modes in sparse packings [as in Fig. 5(b)], we can make clear the qualitative observation that low-frequency modes are often localized to such linear structures. A transverse fluctuation of such a particle (i.e., movement perpendicular to the local bonds) produces a highly localized, low-energy (and low-frequency) vibrational mode. Such an observation is consistent with work characterizing the boson peak frequency $\omega^\star$ in glassy packings as an upper limit of transverse modes [9,45,46]. Under this assumption, the low-area fraction emergence of poorly coordinated structures susceptible to localized transverse vibrational modes would only affect the shape of the vDOS curve below a characteristic frequency, as seen in Fig. 3(a). However, we note that these structures do not account for all highly localized modes in the packings, and not all particles with a locally linear structure contribute to highly localized, low-frequency modes. Thus, the structural origin of these modes must be a bit more complicated than this simple picture.

With the crossover behavior found in the vDOS in mind, we revisit the nearest neighbor data in Fig. 1(h) to explore if there is possibly a hint of that transition in the structural parameter $\overline{NN}$. Therefore, we fit the low- and high-volume fraction data, respectively, with two different lines. In this case, a change in "slope" of $\overline{NN}$ with respect to volume fraction would signal the crossover region. To this end, we determined best-fit lines for data above and below $\phi = 0.67$, and when all data are used, the slopes are 3.1 ± 0.6 (above) and 1.7 ± 1.5, respectively [solid and dotted lines in Fig. 1(h)]. Based on these fits, a hint of a crossover could exist, but it is hard to argue that a crossover region is discovered by the analysis, given the large error bars. If we remove the data point at $\phi = 0.57$, then the case for crossover behavior is strengthened (i.e., the slope for $\phi < 0.67$ becomes 1.4 ± 0.3). Similarly, if we remove only the data point at $\phi = 0.50$, as might be suggested from our analysis of the void distributions [see Fig. 2(d)], then the case for crossover behavior is weakened (i.e., the slope for $\phi < 0.67$ becomes 2.7 ± 1.7) and all data points can be readily fitted to a single line with very small error (3.1 ± 0.4). On balance, however, it is difficult to justify removing data, especially when so few data points are available for the analysis. Thus, though the presented $\overline{NN}$ data are marginally suggestive of a crossover transition, more work with better statistics is needed to reach a definitive conclusion based on nearest neighbor number data.

IV. CONCLUSIONS

In summary, decreasing the area fraction of a quasi-two-dimensional packing of attractive colloidal particles appears to produce a crossover from packings with a glassy distribution of vibrational modes to packings with a gel-like distribution. The crossover from glassy to sparse gel-like states is suggested by an excess of phonon modes at low frequency and by a variation in the slope of the vDOS with frequency also at low frequency. This change in phonon mode distribution is demonstrated to arise largely from localized vibrations that involve individual and/or small clusters of particles with few local bonds. Conventional order parameters and void statistics did not exhibit obvious signatures of a crossover between "gel-like" and "glassy" states as a function of volume fraction. These mode behaviors, and accompanying structural insights, offer a potentially new set of indicators for identification of glass-gel transitions and/or for assignment of gel-like versus glass-like character to a disordered solid material.

In the future, experiments should consider the implications of these results. For example, previous work has correlated spatially localized modes to rearrangement-prone regions in disordered packings [12–17]; this work suggests that an increase in localized low-frequency phonon modes should correlate with a significant change in macroscopic rheological properties of the system. Future experimental studies might

explore if and how this low-frequency vibrational behavior relates to glassy and gel-like bulk rheological features. Additionally, the maximal packing fraction at which the localized modes and microstructures characteristic of gel-like packings arise could depend strongly on the dimensionality and morphology of the system. It is thus important to explore the generalizability of this result to packings with attractive interparticle interactions of varying range, strength, and shape. The present research lays some groundwork for exploring open questions about the nature of glasses and gels, but from a different perspective based on phonon modes.

ACKNOWLEDGMENTS

We thank Andrea Liu, Piotr Habdas, and Peter Collings for useful discussions. This work is supported by the National Science Foundation through NSF Grants No. DMR12-05463, No. DMR12-06231 and the PENN MRSEC Grant No. DMR11-20901, as well as by NASA through Grant No. NNX08AO0G. C.P.G. and D.M.S. also acknowledge support from the U.S. Department of Energy, Office of Basic Energy Sciences, Division of Materials Sciences and Engineering under Award No. DE-FG02-05ER46199.

[1] E. Zaccarelli, J. Phys.: Condens. Matter **19**, 323101 (2007).
[2] P. J. Lu, E. Zaccarelli, F. Ciulla, A. B. Schofield, F. Sciortino, and D. A. Weitz, Nature (London) **453**, 499 (2008).
[3] M. Kroon, W. L. Vos, and G. H. Wegdam, Phys. Rev. E **57**, 1962 (1998).
[4] L. A. Hough, M. F. Islam, B. Hammouda, A. G. Yodh, and P. A. Heiney, Nano Lett. **6**, 313 (2006).
[5] A. J. Liu and S. R. Nagel, Ann. Rev. Condens. Matter Phys. **1**, 347 (2010).
[6] G. L. Hunter and E. R. Weeks, Rep. Prog. Phys. **75**, 066501 (2012).
[7] M. D. Ediger and P. Harrowell, J. Chem. Phys. **137**, 080901 (2012).
[8] C. S. O'Hern, L. E. Silbert, A. J. Liu, and S. R. Nagel, Phys. Rev. E **68**, 011306 (2003).
[9] L. E. Silbert, A. J. Liu, and S. R. Nagel, Phys. Rev. Lett. **95**, 098301 (2005).
[10] M. Wyart, S. Nagel, and T. Witten, Europhys. Lett. **72**, 486 (2005).
[11] K. Chen, W. Ellenbroak, Z. Zhang, D. Chen, P. Yunker, S. Henkes, C. Brito, O. Dauchot, W. van Saarloos, A. Liu *et al.*, Phys. Rev. Lett. **105**, 025501 (2010).
[12] C. Brito and M. Wyart, J. Stat. Mech. (2007) L08003.
[13] A. Widmer-Cooper, H. Perry, P. Harrowell, and D. R. Reichman, Nat. Phys. **4**, 711 (2008).
[14] C. Brito and M. Wyart, J. Chem. Phys. **131**, 024504 (2009).
[15] M. L. Manning and A. J. Liu, Phys. Rev. Lett. **107**, 108302 (2011).
[16] K. Chen, M. L. Manning, P. J. Yunker, W. G. Ellenbroek, Z. Zhang, A. J. Liu, and A. G. Yodh, Phys. Rev. Lett. **107**, 108301 (2011).
[17] A. Ghosh, V. Chikkadi, P. Schall, and D. Bonn, Phys. Rev. Lett. **107**, 188303 (2011).
[18] J. Bergenholtz and M. Fuchs, Phys. Rev. E **59**, 5706 (1999).
[19] L. Fabbian, W. Gotze, F. Sciortino, P. Tartaglia, and F. Thiery, Phys. Rev. E **59**, R1347 (1999).
[20] A. Latka, Y. Han, A. M. Alsayed, A. B. Schofield, A. G. Yodh, and P. Habdas, Europhys. Lett. **86**, 58001 (2009).
[21] T. Eckert and E. Bartsch, Phys. Rev. Lett. **89**, 125701 (2002).
[22] K. N. Pham, A. M. Puertas, J. Bergenholtz, S. U. Egelhaaf, A. Moussaid, P. N. Pusey, A. B. Schofield, M. E. Cates, M. Fuchs, and W. C. K. Poon, Science **296**, 104 (2002).
[23] A. Coniglio, T. Abete, A. de Candia, E. Del Gado, and A. Fierro, J. Phys.: Condens. Matter **20**, 494239 (2008).
[24] L. Rovigatti, W. Kob, and F. Sciortino, J. Chem. Phys. **135**, 104502 (2011).
[25] N. Koumakis and G. Petekidis, Soft Matter **7**, 2456 (2011).
[26] E. Zaccarelli and W. Poon, Proc. Natl. Acad. Sci. USA **106**, 15203 (2009).
[27] A. Zaccone, H. Wu, and E. Del Gado, Phys. Rev. Lett. **103**, 208301 (2009).
[28] A. Eberle, R. Castaneda-Priego, J. Kim, and N. Wagner, Langmuir **28**, 1866 (2012).
[29] D. Beysens and T. Narayanan, J. Stat. Phys. **95**, 997 (1999).
[30] P. J. Yunker, K. Chen, Z. Zhang, and A. G. Yodh, Phys. Rev. Lett. **106**, 225503 (2011).
[31] P. Yunker, Z. Zhang, M. Gratale, K. Chen, and A. Yodh, J. Chem. Phys. **138**, 12A525 (2013).
[32] Z. Zhang, P. J. Yunker, P. Habdas, and A. G. Yodh, Phys. Rev. Lett. **107**, 208303 (2011).
[33] X. Sun, Y. Li, T. H. Zhang, Y.-q. Ma, and Z. Zhang, Langmuir **29**, 7216 (2013).
[34] J. Crocker and D. Grier, J. Colloidal Interface Sci. **179**, 298 (1996).
[35] See Supplemental Material at http://link.aps.org/supplemental/10.1103/PhysRevE.90.062305 for further details about void analysis, mean square displacement, and the vDOS curves.
[36] A. Ghosh, V. K. Chikkadi, P. Schall, J. Kurchan, and D. Bonn, Phys. Rev. Lett. **104**, 248305 (2010).
[37] D. Kaya, N. Green, C. Maloney, and M. Islam, Science **329**, 656 (2010).
[38] S. Henkes, C. Brito, and O. Dauchot, Soft Matter **8**, 6092 (2012).
[39] M. Schindler and A. Maggs, Soft Matter **8**, 3864 (2012).
[40] K. Chen, T. Still, S. Schoenholz, K. B. Aptowicz, M. Schindler, A. C. Maggs, A. J. Liu, and A. G. Yodh, Phys. Rev. E **88**, 022315 (2013).
[41] M. D. Gratale, P. J. Yunker, K. Chen, T. Still, K. B. Aptowicz, and A. G. Yodh, Phys. Rev. E **87**, 052301 (2013).
[42] T. Still, C. P. Goodrich, K. Chen, P. J. Yunker, S. Schoenholz, A. J. Liu, and A. G. Yodh, Phys. Rev. E **89**, 012301 (2014).
[43] M. Wyart, L. E. Silbert, S. R. Nagel, and T. A. Witten, Phys. Rev. E **72**, 051306 (2005).
[44] V. K. de Souza and P. Harrowell, Phys. Rev. E **80**, 041503 (2009).
[45] H. Shintani and H. Tanaka, Nat. Mater. **7**, 870 (2008).
[46] S. Taraskin and S. R. Elliott, Phys. B (Amsterdam, Neth.) **316–317**, 81 (2002).